PCCP

Accepted Manuscript

ROYAL SOCIETY OF CHEMISTRY

www.rsc.org/pccp

Physical Chemistry Chemical Physics
CREATED USING THE RSC LaTeX PCCP ARTICLE TEMPLATE – SEE www.rsc.org/electronicfiles FOR DETAILS
ARTICLE TYPE www. rsc.org/xxxxxx | XXXXXXXX

Complexation of DNA with ruthenium organometallic compounds : the high complexation ratio limit

Stéphane Despax,[a] Fuchao Jia,[a] Michel Pfeffer,[b] and Pascal Hébraud*[a]

Received Xth XXXXXXXXXX 20XX, Accepted Xth XXXXXXXXX 20XX
First published on the web Xth XXXXXXXXXX 200X
DOI: 10.1039/b000000x

Interactions between DNA and ruthenium organometallic compounds are studied by using visible light absorption and circular dichroism measurements. A titration technique allowing for the absolute determination of the advancement degree of the complexation, without any assumption about the number of complexation modes is developed. When DNA is in excess, complexation involves intercalation of one of the organometallic compound ligands between DNA base pairs. But, in the high complexation ratio limit, where organometallic compounds are in excess relative to the DNA base pairs, a new mode of interaction is observed, in which the organometallic compound interacts weakly with DNA. The weak interaction mode moreover develops when all the DNA intercalation sites are occupied. A regime is reached in which one DNA base pair is linked to more than one organometallic compound.

1 Introduction

Metal complexes have been developed for their anticancer activity. Among them, cisplatin[1] and cisplatin-derivated compounds are the mostly used, but they exhibit strong toxicity and are applicable only to a narrow range of tumors[2,3]. For these reasons, other metal-based compounds, in particular ruthenium derivatives, have been synthesized and tested against cancer cell lines[4,5]. Some of them exhibit strong efficiency and much lower toxicity than platinum-based compounds and two of them, NAMI-A[6] and KP1019[7], entered clinical trials. These compounds, as most of the ruthenium compounds described in the literature, are built up with ligand that are relatively weakly bound to the metal *via* a coordination heteroatom-metal bond. In contrast, we have synthesized several ruthenium-based complexes in which one of the ligands is bound to the metal *via* a metal-carbon bound that was further stabilized by an intramolecular N-Ru bond[8]. The stability of this cycloruthenated unit ensures the attachment of the ligand to the metal and enhances the biological activity of the complex. These molecules are called ruthenium-derived compounds (RDC) and it has been shown that several RDCs are cytotoxic *in vitro* for several cancer cell lines that are sensitive or resistant to cisplatin[8]. It has been proposed that the activity of these molecules implies, *inter alia*, their interaction with DNA. It is thus of interest to study their affinity with DNA and elucidate the structure of the formed compounds. Moreover, the localization of RDCs inside cells is heterogeneous : it is strongly localized in and around the nucleus. As a consequence, the local concentration of RDC that controls its reaction with DNA may be noticeably different from its average concentration.

The goal of this paper is to study the interaction of RDCs with DNA in a wide range of DNA/RDC ratios, even when RDC concentration exceeds that of DNA base pairs. The interaction of ruthenium-based compounds with DNA has been studied in the limit of smaller concentrations of ruthenium derivatives than DNA base pairs. Luminescence studies have shown that ruthenium complexes exhibit high affinity with DNA and this technique can allow to recognize specific DNA sequences[9,10]. Several tools have been used to study the interaction between DNA and organometallic molecules : spectroscopic measurements, such as absorption[11] or emission spectroscopy[12–14], dichroic activity, either circular[15], that uses the chiral properties of DNA and of studied complexes or linear[16], by orientation of long DNA double strands under flow, electrochemistry measurements[17], as well as single molecule manipulations[18,19]. The goal of such studies is to follow the association equilibrium between DNA and a small ligand[20,21]. At low ruthenium compound concentrations, the equilibrium may be described by a single adsorption equilibrium :

$$\mathrm{L} + \mathrm{pDNA}_{bp} \underset{K_a}{\rightleftharpoons} (L - pDNA_{bp})$$

so that the equilibrium is characterized not only by the affinity constant of the ligand with DNA but also by the number of DNA base pairs involved in a single ligand molecule adsorption[22]. In the case where the number of base pairs p is large enough so that steric effects cannot be neglected, one needs to

[a] *IPCMS/CNRS, Université de Strasbourg, UMR 7504 23 rue du Loess, 67034 Strasbourg*
[b] *Institut de Chimie, CNRS, UMR7177, Université de Strasbourg.*

take into account that uncomplexed DNA base pairs belonging to a succession of uncomplexed base pairs whose length is smaller than p are no longer available for further complexation [23].

Contrary to cisplatin, DNA association with ruthenium complexes does not involve the formation of a covalent bond and the structure of the DNA/RDC compound is unknown. Several interactions have been established for these complexes [11] :

- interaction of one of the ligands of the ruthenium complex between DNA base pairs. The intercalation may be total or partial. In that case, only a part of the ligand intercalates between the DNA base pairs [13,15,16,24],
- surface interaction, in which the complex interacts with the major or the minor DNA groove through van der Waals interaction [12],
- lastly, electrostatic interaction between the complex and the DNA phosphate backbone [12,25].

Depending on the ruthenium compound under study, one or the other type of interactions plays a dominant role, and leads to a particular DNA-RDC structure. Moreover, depending on the relative amount of DNA base pairs and ligands, the complexation may lead to different structures [26]. Moreover, DNA being a chiral molecule the two enantiomers of a given complex may exhibit different affinities towards DNA [12,27–29].

In this paper, we focus our attention on a complex that has been proven to possess a high anticancer activity [30]. It consits in the association between ruthenium (II) and three monoanionic or neutral bidentate ligands. One of them is an aryl-2-pyridine ligand that binds to the ruthenium atom through a covalent bond Ru-C and a coordination bond Ru-N. The two remaining ligands bind to the metal through coordination bonds. One closely related molecule will also be studied : RDC40Cl, where an electron acceptor group (NO_2) is added to the phenylpyridine ligand (fig. 1).

Absorption as well as circular dichroism are performed. We characterize the change of RDC absorbance when complexation with DNA occurs. Titrations of RDC with DNA are thus performed in which the evolution of the maximum of absorption is monitored. We concentrate our analysis on the relationship between the variation of the molar absorbance and the ratio of complexation of DNA by RDC. As the molar absorbance of the pure compound consisting of RDC linked to DNA is unknown and cannot be determined, a model needs to be developed. Although the principal value analysis [31] may be used, it does not allow for the determination of the spectral properties of the adsorbed complex. We thus have chosen to generalize a technique developed by Nishida [32] and Bujalowski [33], in which two titrations are performed at two different concentrations. Assuming that if the same change of

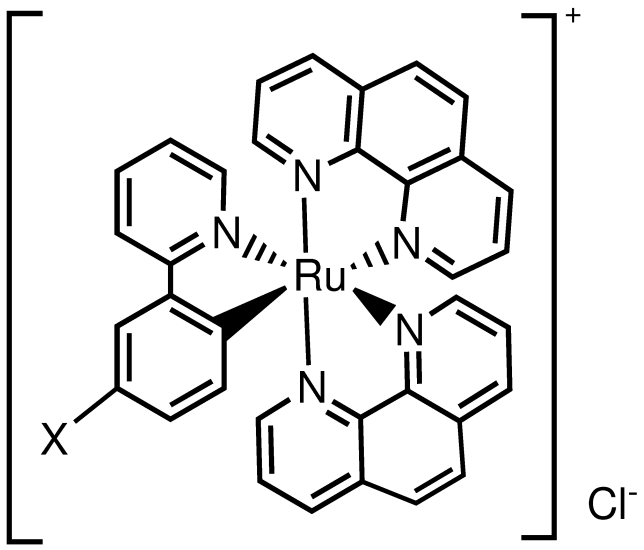

Fig. 1 Molecular structure of the studied ruthenium complexes. RDC37Cl : X=H ; RDC40Cl : X= NO_2.

absorbance per DNA base pair is measured at two different DNA concentrations, then, the ratio of complexed DNA sites is the same, one can thus deduce this fraction from these measurements. It has been shown by Bujalowski [33] that this technique is very efficient in the case where one equilibrium is at play. We will extend this technique to consider the case of two different complexation equilibria.

2 Materials and methods

2.1 Absorption Spectrophotometry

Absorption spectra are performed with a Uvikon XL spectrophotometer from BIO-TEK Instruments, in specific absorption cuves ($800\mu L$ in volume) of 1 cm optical path. Ruthenium complexes possess two main characteristic absorption bands : a UV band ($200-400$nm) corresponding to $\pi-\pi^*$ (LC) transitions and a visible band ($400-800$nm) due to MLCT transitions. We determine the λ_{max} absorption due to the MLCT transition by registering the absorption spectra between 400 and 800nm. λ_{max} is approximately equal to 475 nm. At this wavelength, the absorbance of DNA (salmon sperm, sheared 10 mg/mL from Invitrogen) is negligible and the measured signal is entirely due to the MLCT band of the ruthenium compound. Absorption is first studied as a function of the RDC concentration and was found to linearly increase up to $\approx 10^{-4}$ M. For the RDC studied, the concentration were thus chosen between $2\text{x}10^{-5}$ and $8\text{x}10^{-5}$ M. All the solutions, DNA and RDC, were prepared in distilled water without any salt or

buffer. For the titration, the DNA solution concentrations was 1mg/mL and then, amounts of DNA were added to the RDC solution and the evolution of the 475 nm absorption band is monitored from a ratio of DNA base pairs concentration over RDC concentration, $[DNAbp]/[RDC]$ from 10^{-1} to 10. A ratio increase of 0.1 corresponds to a DNA amount of 1.07 μL for a RDC solution at 2x10^{-5} M.

2.2 Circular Dichroism

CD spectra were performed on J810 apparatus from Jasco in specific cuvettes (3 mL volume) of 1 cm optical path, between 220 and 500 nm. The absence of CD signal for a RDC racemic solution (2x10^{-5} M) was verified. Background signal, arising from the solvent and the cuvette of solvent is substracted from each measurement. Modification of the mixture signal was monitored with increasing amounts of DNA (salmon sperm from Invitrogen) solution (1 mg/mL). All the solutions, RDC and DNA, were prepared in distilled water without any salt or buffer. For the titration, additions of DNA amounts were performed from a ratio $\frac{[DNAbp]}{[RDC]}$ from 0.1 to 10. A ratio increase of 0.1 corresponds to a DNA amount of 4 μL for a RDC solution at 2x10^{-5} M.

2.3 Synthesis

The NMR spectra were obtained at room temperature on a Brucker spectrometer. ^{1}H NMR spectra were recorded at 500.13 (AM-500) and referenced to $SiMe_4$. The chemical shifts are referenced to the residual solvent peak. Chemical shifts (δ) and coupling constants (J) are expressed in ppm and Hz respectively. Multiplicity: s = singulet, d = doublet, t = triplet, m = multiplet.

Elemental analyses were carried out by the available facilities at the Institut de Chimie of the Université de Strasbourg.

Experiments were carried out under an argon atmosphere using a vacuum line. Diethyl ether and pentane were distilled over sodium/benzophenone, dichloromethane and acetonitrile over calcium hydride and methanol over magnesium under argon immediately before use. Chromatography columns were carried out on Merk aluminium oxide 90 standardized. The other starting materials were purchased from Sigma-Aldrich or Alfa Aesar and used as received without further purification.

Compounds RDC37[34], $[Ru(bpy)_2(dppz)]^{2+}(BF4^-)_2$[35,36] and RDC37Cl[37] were synthesised according to published procedures.

Whilst we checked that the ^{1}H NMR spectrum of RDC37Cl in CD_3CN was identical to that of RDC37, we found that an important signal of water was present at 2.15 ppm. Recrystallisation of the compound in CH_3CN/Et_2O (that afforded deep red crystals) followed by prolonged drying of this compound under vacuum did not modify the amount of water present. The combustion analysis (that was apparently not performed[38]) confirmed the presence of 3 molecules of water per molecule of RDC37Cl; $[C_{35}H_{30}ClN_5O_3Ru]$ (RDC37Cl, 3 H_2O) calcd : C = 59.61, H = 4.29, N = 9.93; found: C = 59.90, H = 4.50, N = 9.25.

RDC40

This synthesis follows the procedure[30] used to obtain the closely related compound having a triflate as counter-anion. To a deep purple solution of RDC37 (410mg, 0.54 mmol) in 40 ml of CH_2Cl_2, was added $AgNO_3$ (93 mg, 0.55 mmol), and $PhCOCl$ (62.5 μl, 0.54 mmol). The solution was stirred at room temperature for 18 hours. TLC revealed only a red spot wich was collected by column chromatography over Al_2O_3 using CH_3CN as eluent and concentrated *in vacuo*. The resulting powder was dissolved in the minimum amount of CH_3CN (*ca* 10mL) and after the addition of Et_2O (*ca* 100mL) a dark red solid precipitated of mass 390 mg. Yield : 90 %.

^{1}H NMR (500 MHz, CD_3CN): δ= 8.64 (d, 1H, $^4J_{HH}$=2.3), 8.52 (dd, 1H, $^3J_{HH}$=8.2, $^4J_{HH}$=1.4), 8.44 (dd, 2H, $^3J_{HH}$=8.1, $^4J_{HH}$=1.1), 8.38 (dd, 1H, $^3J_{HH}$=8.2, $^4J_{HH}$=1.2), 8.33 (dd, 1H, $^3J_{HH}$=5.2, $^4J_{HH}$=1.2), 8.24 (d, 1H, $^3J_{HH}$=8.4), 8.18 (m, 1H), 8.16 (d, 2H, $^3J_{HH}$=4.0, 2H), 8.12 (d, 2H, $^4J_{HH}$=1.1, 2H), 8.06 (dd, 1H, $^3J_{HH}$=5.0, $^4J_{HH}$=1.4), 7.86 (dd, 1H, $^3J_{HH}$=5.2, $^4J_{HH}$=1.1), 7.75 (t, 1H, $^3J_{HH}$=7.8), 7.66-7.62 (m, 3H), 7.60 (dd, 1H, $^3J_{HH}$=8.2, $^4J_{HH}$=5.3), 7.48 (dd, 1H, $^3J_{HH}$=8.4, $^4J_{HH}$=2.4), 7.45 (dd, 1H, $^3J_{HH}$=8.2, $^4J_{HH}$=5.5), 6.94 (ddd, 1H, $^3J_{HH}$=7.2, $^3J_{HH}$=5.6, $^4J_{HH}$=1.2), 6.64 (d, 1H, $^3J_{HH}$=8.4).

This compound was used as such without further purification to obtain the corresponding chloro derivative, RDC40Cl.

RDC40 (100 mg, 0.12 mmol) was deposited on a column of Amberlite® IRA-400 (50g) (that was previously activated according to the procedure described in ref[38]) using 4 mL of acetone, and eluted with MeOH. The coloured solution contained the product. Evaporation of the solvent in vacuo quantitatively gave RDC40Cl as a deep red solid (90 mg). The procedure was repeated 3 times in order to eliminate any trace of PF_6^- containing compound.

The ^{1}H NMR of this product was also exactly the same as that of its precursor with, as for RDC37Cl, the existence of water at 2.15 ppm. Here also, recrystallisation of the compound in CH_3CN/Et_2O (that afforded deep red crystals) followed by prolonged drying under vacuum did not significantly modify the amount of water present. The combustion analysis confirmed the presence of 5 molecules of water per molecule of RDC40Cl; [$C_{35}H_{30}ClN_5O_7Ru$] (**RDC40Cl**, 5 H_2O) calcd : C = 53.47, H = 4.23, N = 10.69; found: C = 53.80, H = 3.80, N = 10.40.

3 Absorption study

Our purpose is to study and quantify the association between a double stranded DNA macromolecule and organometallic ruthenium complexes. The thermodynamic description of the equilibrium is more complex than an equilibrium between small molecules. Indeed, the DNA helix may bind with several RDC molecules, each of them occupying an *a priori* unknown number of DNA base pairs along the chain. We will call each sequence of DNA base pairs of such length a "site". Several modes of complexation (intercalation, groove binding through one or several chelate groups[26]) may coexist.

3.1 Equilibria in competition

In a first approximation, let us assume that the equilibrium between DNA macromolecule and RDC drug is described by :

$$\mathrm{S} + \mathrm{RDC} \overset{K_{a1}}{\rightleftharpoons} (\mathrm{S}-\mathrm{RDC})_1$$
$$\mathrm{S} + \mathrm{RDC} \overset{K_{a2}}{\rightleftharpoons} (\mathrm{S}-\mathrm{RDC})_2$$

where S is an association site consisting of p DNA base pairs whose total concentration is S_t, (S - RDC)$_1$ and (S - RDC)$_2$ are complexed sites with conformation 1 or 2.

Due to local modifications of the electron density when the RDC complex is associated with DNA, absorbance of RDC's MLCT band decreases with increasing DNA base pairs concentration (fig. 2). The transition probability, directly related to the electronic density, is quantified by the molar absorbance, ε. The ε value evolves from ε_f from a free complex to ε_b for a bound RDC complex. When different modes of complexation coexist, the molar obsorbance of bound RDC can take two values, ε_{b1} and ε_{b2}. The total absorbance A_{obs} (at λ_{max} of MLCT absorbance) is the sum of the absorbance of the free and bound ligands, A_f and A_b :

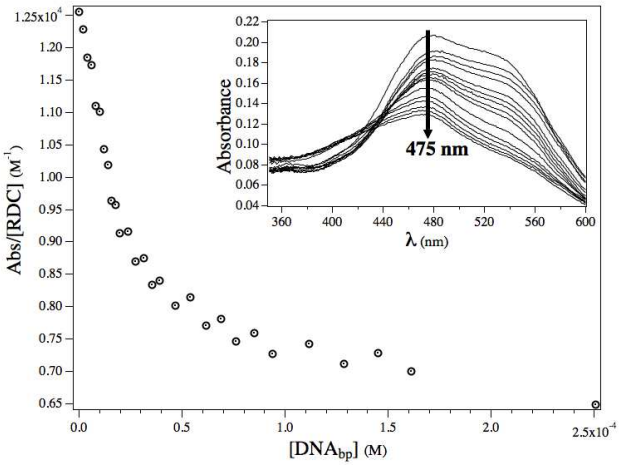

Fig. 2 Absorbance spectra of solutions of RDC37Cl ($2\text{x}10^{-5}$ mol.L^{-1}) with increasing concentration of DNA from top to bottom (0 to 10^{-4} mol.L^{-1}). *Insert :* Evolution of the absorbance of the solution at $\lambda = 475$ nm as a function of the concentration of added base pairs of DNA, D_t.

$$\begin{aligned} A_{obs} &= A_f + A_b = \varepsilon_f L_f + \varepsilon_{b1} L_{b1} + \varepsilon_{b2} L_{b2} \\ &= \varepsilon_f (L_t - (L_{b1} + L_{b2})) + \varepsilon_{b1} L_{b1} + \varepsilon_{b2} L_{b2} \end{aligned} \quad (1)$$

where L_f is the concentration of free ligands, and L_{b1}, L_{b2} are the concentrations of bound ligands according to modes 1 and 2. In this equation, the molar absorbance is expressed as the inverse of a concentration (M^{-1}) in all the following development. Assuming that ε_{b1} and ε_{b2} are known from independent measurements and using the mass action laws for the two equilibria, the measurement of the absorbance allows for the determination of the advancement degrees of the equilibria. Nevertheless, in our case, and in many other situations, ε_{b1} and ε_{b2} cannot be measured independently. We thus develop a titration protocol that releases us from the knowledge of the molar absorbances of the bound states. The central quantity of this protocol will be the absorption change *per* mole of DNA adsorption site :

$$Q^S_{obs} = \frac{A_{obs} - \varepsilon_f L_t}{S_t} \quad (2)$$

3.2 Analysis method of the titration

Let us first remark that, as a consequence of the mass action laws, the ratio of occupied sites according to mode 1 or 2 ν^S_2/ν^S_1 is equal to the ratio between affinity constants, K_{a2}/K_{a1}. Considering the absorption change *per* mole of DNA adsorption site, $Q^S_{obs} = \frac{A_{obs} - \varepsilon_f L_t}{S_t}$, we obtain :

$$Q^S_{obs} = \nu^S \times \left(\frac{\varepsilon_{b1} + \varepsilon_{b2}\alpha}{\alpha + 1} - \varepsilon_f \right) = \nu^S \times \tilde{\Delta\varepsilon} \quad (3)$$

$\alpha = K_{a2}/K_{a1}$ is the ratio of the complexation constants and $\tilde{\Delta\varepsilon} = \left(\frac{\varepsilon_{b1} + \varepsilon_{b2}\alpha}{\alpha+1} - \varepsilon_f \right)$ is the weighted average of the variation of molar absorbance of RDC at λ_{max} upon complexation with DNA. By dividing this relationship by the occupation site size p, we get a similar equation from DNA base pairs concentration value :

$$Q^D_{obs} = \frac{A_{obs} - \varepsilon_f L_t}{D_t} = \nu^D \times \tilde{\Delta\varepsilon} \quad (4)$$

$\tilde{\Delta\varepsilon}$ is a function of molar absorbances of bound compounds, ε_{b1} and ε_{b2}, of free compounds, ε_f, and of the affinity constants K_{a1} and K_{a2}, but does not depend on the advancement degree of the complexation, ν^D. We cannot determine $\tilde{\Delta\varepsilon}$, as it would require the measurement of the absorbance of DNA

saturated with RDC and the *a priori* knowledge of K_{a2}/K_{a1}. As already stated, the saturation cannot be reached due to the low solubility of RDC.

We thus now develop a procedure that allows the complete study of the complexation. Following [33], we now perform two titrations at two different initial ruthenium complex concentrations, L_t and L'_t. Along each titration, one has $Q^S_{obs} = \nu^S \tilde{\Delta\varepsilon}$ and $Q'^S_{obs} = \nu'^S \tilde{\Delta\varepsilon}$, where the weighted average of molar absorbances, $\tilde{\Delta\varepsilon}$ does not depend on the concentrations and advancement degrees of the reaction. As a consequence, two points of the two titration curves (fig 3) that exhibit the same absorbance *per* mole of DNA, $Q^S_{obs} = Q'^S_{obs}$ correspond to the same complexation ratios, $\nu^S = \nu'^S$. Moreover, the equilibrium is satisfied at any point along the titrations :

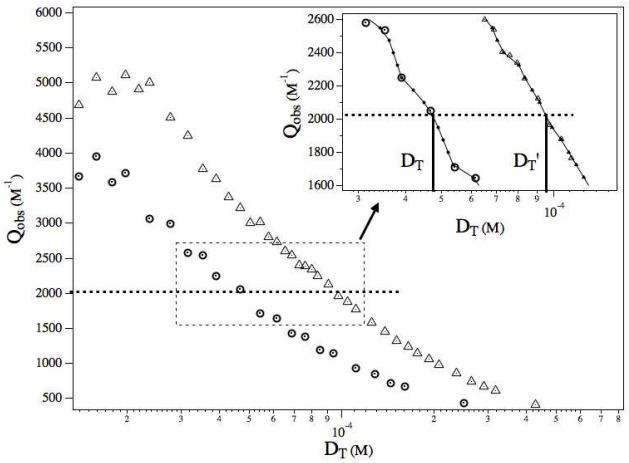

Fig. 3 Experimental determination of the fraction of adsorbed DNA sites. The variation of absorbance per mole of DNA base pairs is measured along two titrations of RDC at two concentrations, L_t (◯) and L'_t (△). Values of DNA base pairs concentration corresponding to a given value are obtained using a linear approximation between successive experimental measurements (see *insert*, filled symbols are experimental results, empty circles correspond to linear approximation for a series of values of Q^D_{obs}). From D_t and D'_t values, one obtains the fraction of adsorbed sites, ν^S using eq. 9. The two experimental curves chosen to illustrate the technique are obtained for RDC37Cl with $L_t = 2\text{x}10^{-5}$ M (◯) and $L'_t = 4\text{x}10^{-5}$ M (△).

$$K_{a2}/K_{a1} = \nu^S_2/\nu^S_1 \quad (5)$$
$$K_{a2}/K_{a1} = \nu'^S_2/\nu'^S_1 \quad (6)$$

where $\nu^S = \nu^S_1 + \nu^S_2$ and $\nu'^S = \nu'^S_1 + \nu'^S_2$. As a consequence, $\nu^S_1 = \nu'^S_1$ and $\nu^S_2 = \nu'^S_2$. But the mass action laws write :

$$K_{a1} = \frac{L_{b1}}{S_f L_f} = \frac{\nu^S_1}{(1-(\nu^S_1+\nu^S_2))L_f} \quad (7)$$
$$K_{a1} = \frac{L'_{b1}}{S'_f L'_f} = \frac{\nu'^S_1}{(1-(\nu'^S_1+\nu'^S_2))L'_f} \quad (8)$$

so that two points along the two titration curves where $Q^S_{obs} = Q'^S_{obs}$ correspond to the same free ligands concentrations, $L_f = L'_f$.

The fraction of adsorbed sites are thus obtained from the conservation of matter :

$$\left.\begin{aligned} L_t &= L_f + \nu^S S_t \\ L'_t &= L'_f + \nu'^S S'_t \end{aligned}\right\} \quad \Longrightarrow \quad \nu^S = \frac{L'_t - L_t}{S'_t - S_t} \quad (9)$$

or, by dividing by p, $\nu^D = \frac{L'_t - L_t}{D'_t - D_t}$.
This reasoning leads to an experimental procedure to measure ν^D : Q^D_{obs} is measured experimentally for two different RDC concentrations, L_t and L'_t. The total DNA concentrations along each titration corresponding to the same Q^D_{obs} are then determined, from which ν_D is computed, using eq. 9 (fig. 3).
The slope of Q^D_{obs} as a function of ν^D leads to the variation of molar absorbance, $\tilde{\Delta\varepsilon}$ (fig. 4).

3.3 Results

Considering RDC37Cl (fig. 4a), we observe that Q^D_{obs} is not simply proportional to the DNA base pairs occupation, ν^D. Two linear domains may be defined : the slope is higher at low ν^D than at large ν^D values. We define ν^D_c the cross-over value of ν^D between the two regimes. This non linearity has strong implications :

- the adsorption of RDC onto DNA occurs through two different modes of complexation,
- these two modes are associated with two different adsorption sites. The most affine sites may reach saturation while complexation still proceeds onto the least affine ones. This leads to the shoulder in the $Q^D_{obs}(\nu^D)$ curve. On the opposite, if the two complexation would occur onto the same sites, the equilibrium would be described by eq. 4 and a linear behavior whose slope is given by a weighted average of the molar absorption change would be obtained, up to the saturation of sites.

Moreover, ν^D values may moreover be larger than 1, which means that more than one RDC molecule complexes with one DNA base pair. Conversely, the evolution of Q^D_{obs} in the case of RDC40Cl (fig. 4b) molecule exhibits a linear relationship,

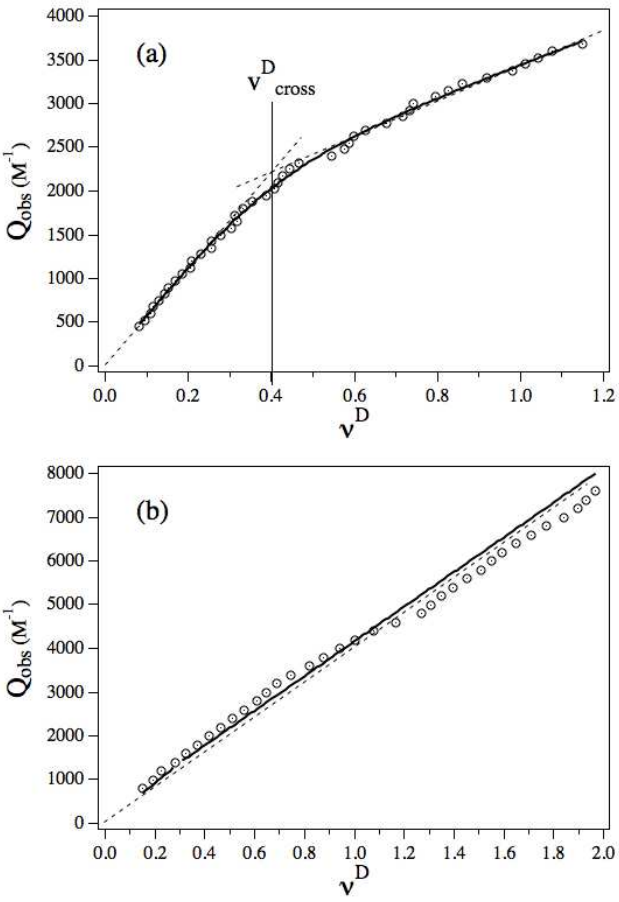

Fig. 4 Evolution of Q^D_{obs} as a function of the fraction of occupied DNA base pairs, ν^D. Results are given for the two studied ruthenium compounds : **(a)** RDC37Cl and **(b)** RDC40Cl. Dashed lines are linear fits of the asymptotic behaviors at low and high ν^D from eq. 11. Thick continuous lines are fits according to eq. 13 with K_{a2}/K_{a1} as the sole fitting parameter.

up to ν^D_c values larger than 1. As a single mode of complexation cannot lead to ν^D values larger than 1, in light of the results obtained for RDC37Cl, it may be assumed that two complexation modes also coexist for RDC40Cl. Nevertheless, the molar extinction coefficient is very similar for the two complexation modes.

We come to the conclusion that two different complexation sites, S_1 and S_2, coexist along the DNA chain. They possess different affinities, K_{a1} et K_{a2}, for RDC :

$$S_1 + RDC \overset{K_{a1}}{\rightleftharpoons} (S_1 - RDC)$$
$$S_2 + RDC \overset{K_{a2}}{\rightleftharpoons} (S_2 - RDC)$$

The analysis of the titration assumes that two solutions exhibiting the same absorption variation per mole of association site possess the same fraction of occupied sites. Although this is clearly true when the adsorption is governed by two equilibria in competition, it is not generally true when two kinds of adsorption sites with different affinity constants coexist. Indeed, the same values of Q_{obs} may be obtained with a strong adsorption ratio onto sites leading to small changes of molar absorption or a smaller adsorption ratio onto sites with high changes of molar absorption. As a consequence, the analysis presented above is not general enough and must be validated in our specific situation. The complete analysis is detailed in the Appendix, and we obtain :

$$Q^D_{obs} = \nu^D(\varepsilon_f - \varepsilon_{b2}) + \frac{\nu^D}{1 + \frac{L_{b2}}{L_{b1}}\left(\frac{\nu^D}{\langle p\rangle}\right)}(\varepsilon_{b2} - \varepsilon_{b1}) \qquad (10)$$

where $\langle p\rangle$ is the average of the number of base pairs *per* site. In a first step, ε_{b1} and ε_{b2} values are determined by the slopes of $Q^D_{obs}(\nu^D)$ in the limits $\nu^D \to 0$ and $\nu^D \to \nu^D_{max}$ (dashed lines, fig. 4) :

$$\lim_{\nu^D \to 0} Q^D_{obs}(\nu^D) = \nu^D(\varepsilon_f - \varepsilon_{b1}(\frac{1}{1 + \frac{\phi_2}{\phi_1}\frac{K_{a2}}{K_{a1}}}) - \varepsilon_{b2}(1 - \frac{1}{1 + \frac{\phi_2}{\phi_1}\frac{K_{a2}}{K_{a1}}}))$$
$$\approx \nu^D(\varepsilon_f - \varepsilon_{b1}) \qquad (11)$$
$$\lim_{\nu^D \to \nu^D_{max}} Q^D_{obs}(\nu^D) \approx \nu^D(\varepsilon_f - \varepsilon_{b2}) \qquad (12)$$

Then, the experimental curves are fitted with eq. 13 (continuous lines, fig. 4) with K_{a2}/K_{a1} as the sole parameter, controlling the curvature at $\nu^D = \nu^D_c$.

$$Q^D_{obs} = \nu^D(\varepsilon_f - \varepsilon_{b2}) + \frac{\nu^D}{1 + \frac{L_{b2}}{L_{b1}}(\nu^D)}(\varepsilon_{b2} - \varepsilon_{b1}) \qquad (13)$$

The values are given in Tab. 6.

The two interactions exhibit strong difference of affinities : $K_{a2}/K_{a1} \ll 1$, and the variation of molar absorbance is much higher for the first than for the second interaction mode.

3.4 Determination of K_{a1}

In the low complexation regime, the most affine reaction, 1, controls the equilibrium, and mass action law and the absorbance are :

$$K_{a1} = \frac{L_{b1}}{(S_t - L_{b1})(L_t - L_{b1})} \qquad (14)$$
$$A_{obs} = \varepsilon_{b1}L_{b1} + \varepsilon_f L_f \qquad (15)$$

which may be written as[39] :

$$\frac{S_t L_t}{\Delta A_{obs}} - \frac{S_t + L_t}{\Delta\varepsilon_1} + \frac{\Delta A_o bs}{(\Delta\varepsilon_1)^2} = \frac{1}{K_{a1}\Delta\varepsilon_1} \qquad (16)$$

where $\Delta A_{obs} = A_{obs} - \varepsilon_f L_t$ and $\Delta\varepsilon_1 = \varepsilon_{b1} - \varepsilon_f$. The slope and the value at origin of $\frac{S_t L_t}{\Delta A_{obs}}$ as a function of $S_t + L_t$ then leads to a first approximation of K_{a1} and $\Delta\varepsilon_1$. An iteration procedure is then applied onto the values corresponding to the regime with the highest affinity only (ε_{b1}), and calling $\Delta\varepsilon_{1,n}$ and $K_{a1,n}$ the values found after the nth step, we have :

$$\frac{S_t L_t}{\Delta A_{obs}} + \frac{\Delta A_{obs}}{(\Delta\varepsilon_{1,n})^2} = \frac{1}{K_{a1,n+1}\Delta\varepsilon_{1,n+1}} + \frac{S_t + L_t}{\Delta\varepsilon_{1,n+1}} \qquad (17)$$

from which $\Delta\varepsilon_{1,n+1}$ and $K_{a1,n+1}$ are obtained. A rapid convergence after 5 iterations is obtained (fig. 5), and the obtained values of K_{a1} and ε_{b1} are given in fig. 6.

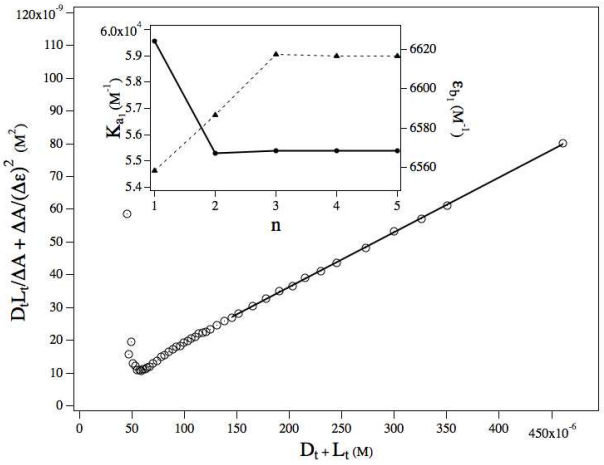

Fig. 5 Hildebrand-Benesi[39] plot of the evolution of the absorbance as a funciton of the total concentration of ligands and base pairs, according to eq. 17 for $n = 5$ iterations. The slope leads to ε_{b1} and one deduces K_{a1} from the value at origin. *Insert* : successive approximations of ε_{b1} and K_{a1} values obtained with the Hildebrand analysis as a function of the number of iterations, n. For all compounds studied, the asymptotic value is reached after a few iterations.

The experimental data used to obtain these values are chose using the Q_{obs} plot : all the points in the first domain are selected and the DNA_{bp} concentrations, RDC concentrations and absorbance values corresponding to these points are used to perform the K_{a1} and ε_{b1} determinations described before. The values of ε_{b1} obtained from the Q_{obs} plot and from the Hildebrand-Benesi analysis (fig. 6) are coherent (around 5% of difference) and show a good correlation between the two methods used (Bujalowsky and Hildebrand-Benesi).

3.5 Discussion

Several association models between DNA and ruthenium chelates have been suggested. For chiral components, the intercalation structure has been observed to depend on the enantiomer under study [40,41]. It has also been observed that a given enantiomer may possess two different modes of association, depending on its concentration relative to the DNA concentration[26]. The intercalation may be partial or complete[42], depending on the angle of intercalation relative to the DNA axis[15]. This leads to different depths of intercalation[16]. Most observations tend to show that the intercalation occurs through the major DNA groove, but recent NMR measurements have shown that association with the minor groove also occurs[43,44]. Raman spectroscopy may allow to determine wich ligand is intercalated between the DNA base pairs[45].

		RDC37Cl		RDC40 Cl	$Ru(bpy)_2(dppz)^{2+}$
		0 mM Nacl	40 mM Nacl		
ε_f		12550	12550	12260	15725
ε_{b1}	$Q_{obs}(\nu)$	6293	5047	7623	13924
	Hildebrand	6568	4523	7663	14101
ε_{b2}		10858	6363		15233
K_{a1}		$5.9\text{x}10^4$	$8\text{x}10^4$	$5.5\text{x}10^5$	$1.1\text{x}10^4$
K_{a2}		$3.5\text{x}10^3$	$4.8\text{x}10^2$		$6.6\text{x}10^4$

Fig. 6 Molar absorbances ε_{b1} in $\text{mol}^{-1}.l$ and affinity constants. K_{a1} ($\text{mol}^{-1}.l$) is obtained from the Hildebrand-Benesi analysis (eq. 17), ε_f ($\text{mol}^{-1}.l$) is obtained from the measurement of the absorbance of a solution of RDC solutions. ε_{b1}, ε_{b2} ($\text{mol}^{-1}.l$) are given by the linear slope of $Q^D_{obs}(\nu^D)$ at low and high ν^D values. $\frac{K_{a2}}{K_{a1}}$ is obtained from the fitting of Q^D_{obs} according to eq. 13 (see fig. 4), from which K_{a2} is obtained

Several modes of complexation thus may exist and have been identified for $Ru(bpy)_2(dppz)^{2+}$ using film voltammetry technique[24]. Let us now identify the nature of the interaction for the two modes observed in our experiments. As we see before, the first domain corresponds certainly to an intercalation mode. To proove this, it is interesting to compare our results to the one obtained for the complexation of DNA with $[Ru(bpy)_2(dppz)]^{2+}$, whose dppz ligand is known to intercalate between DNA base pairs, and that possesses secondary interaction modes.

According to the litterature, this complex is a good intercalator between DNA base pairs[13,46] at very high concentration ratio of DNA base pairs against complex ($\frac{DNA_{bp}}{Ru} > 10$). This compound develops a very high affinity constant with DNA macromolecule : around $10^6\ M^{-1}$ for electrochemical luminescence[17], emission spectroscopy[46], DNA stretching experiments[18] ; around $10^5\ M^{-1}$ for AFM experiment[18]. Raman spectroscopy measurements[45] show that this complex interact through dppz ligand but the aromatic plane is just partially intercalated by the phenazine part. For several years, luminescence experiments on these systems were developped and an important observation was that the luminescence bi-

exponential decreasing time of the ruthenium complex associated with DNA [9]. As a consequence, two kinds of interactions exist, corresponding to two different intercalations with different geometries : the dppz ligand axis may be parallel (side-on geometry) or perpendicular to the DNA macromolecule axis [13]. In our experiments, the variation of the dppz complex absorbance is not very sensitive to the intercalation geometries, so the experimental detection of these two different kinds of intercalation is not detected. However, we observe a new interaction mode at low $\frac{DNA_{bp}}{Ru}$ ratio, *i.e.* when the complex is in excess against DNA base pairs. It is remarkable that $[Ru(bpy)_2(dppz)]^{2+}$ results (fig. 7) are very similar to the RDC complex, two limit domains can be described : the first one at low DNA occupation fraction (< 0.5) corresponding to the intercalation of complex between DNA base pairs (independent of the intercalation geometries), and the second one at high DNA occupation fraction (> 0.5) corresponding to another kind of interaction, possibly surface bounding or electrostatic, with a very lower affinity constant. For the first

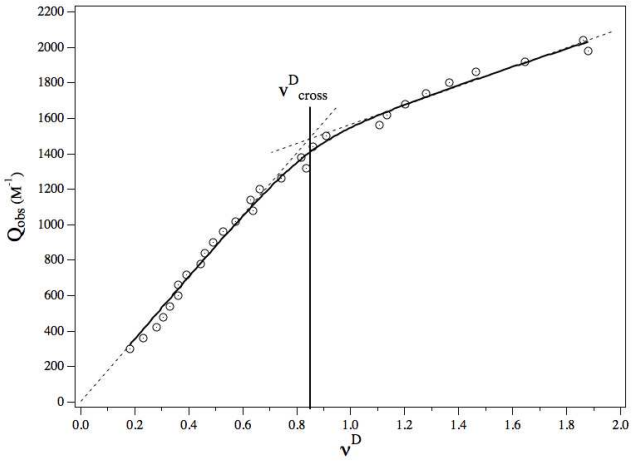

Fig. 7 Evolution of Q^D_{obs} as a function of the fraction of occupied DNA base pairs, ν^D for the compound $[Ru(bpy)_2(dppz)]^{2+}$. Dashed lines are linear fits of the asymptotic behaviors at low and high ν^D from eq. 11. Thick continuous lines are fits according to eq. 13 with K_{a2}/K_{a1} as the sole fitting parameter.

domain and using the Hildebrand-Benesi analysis described before, the $[Ru(bpy)_2(dppz)]^{2+}$ compound show a very high affinity constant, $K_{a1} = 1.1\text{x}10^5\ M^{-1}$, wich is comparable to the litterature values with the assumption of a single equilibrium. So the nature of the interaction for this domain is clearly the intercalation for $[Ru(bpy)_2(dppz)]^{2+}$ and according to the results for the RDC compounds we can assume the same kind of interaction for all the first domain (excess of DNA_{bp}).

But there is a great structural difference between RDC and $[Ru(bpy)_2(dppz)]^{2+}$: the latter possesses a dppz ligand whereas the former is linked with phenanthrolines ligands. The intercalation of phenanthroline ligand has been discuted for several years [16,25] : obviously the phenanthroline ligand interacts less than the dppz ligand considering an intercalation.

The interaction between $[Ru(phen)_3]^{2+}$ and DNA has indeed been studied [16,25] : the phenanthroline ligand intercalates between DNA base pairs, but with a much lower affinity than the dppz ligand. A large part of the work has been focussed on the complex-DNA association enantioselectivity due to the DNA chiral nature [12,40,43,47,48]. Studies have been performed at a very high concentration ratio $\frac{DNA_{bp}}{RDC} > 10$ and it seems that the phenanthroline intercalation is accepted for this range of concentration ratios values [16]. However, the intercalation geometry details are not known and particularly, Δ and Λ isomers do not lead to the same association structure [12,40,43,47,48]. Moreover, DNA structure modification is very low [48] comparing to a classical intercalator as dppz ligand, the most plausible explanation is that the phenanthroline does not intercalate deeply into DNA macromolecule, but just interact through semi or quasi-intercalation [16].

According to the results shown in fig.7, the affinity constant of RDC37Cl in the first domain is lower than the one of $[Ru(bpy)_2(dppz)]^{2+}$: $K_{a1}(\text{RDC37Cl}) = 5.9\text{x}10^4\ M^{-1} < K_{a1}([Ru(bpy)_2(dppz)]^{2+}) = 1.1\text{x}10^5\ M^{-1}$. This difference is probably due to the different depth of the intercalation, the dppz ligand going more into the DNA structure than the phenanthroline ligand. The partial intercalation of the phenanthroline makes it sensitive to other interactions. It may be responsible for the smaller affinity constant of RDC37Cl than that of RDC40Cl. RDC40Cl possesses a NO_2 electronic attractor group that may develop a stabilization interaction with the phosphate anions. Moreover, the electroacceptor effect of NO_2 on the intercalated ligand modifies the electronic density of the intercalated phenanthroline aromatic ring and increases the $\pi - \pi$ stack interaction between this electron deficient ligand and the electron excedent aromatic rings of the DNA base pairs, in particuler pyridine and purine. Both phenomena may explain the higher affinity of RDC40Cl to DNA double strand than RDC37Cl that does not possess an electroacceptor group.

In conclusion, we assume that, at low DNA occupation fraction, the main interaction between DNA and RDC complexes is an intercalation, without considering the different possible association geometries.

For the second domain, the results give a lower affinity constant for all the compounds studied, and the variation of the molar absorbance is too weak to have an intercalation mode. As below, we perform more experiments to study more specifically this second mode.

4 Study of the low interaction mode

To identify the second mode of association we perform others experiments. First, circular dichroism : this manipulation can give some informations about the DNA structure during the titration. Then absorption spectrophotometry, as before, but in saline medium to vary the ionic force of the solution.

4.1 Circular dichroism

The CD signal of B-DNA is very characteristic [49], with a positive band at 275nm and a negative band around 250nm. These bands are assigned to the spatial structure of double strand DNA and to the helical arrangement of the base pairs. A modification of the DNA structure or base pair distances of interaction force induces a change of the CD signal. Circular and linear dichroism spectroscopies have been used to investigate the change of DNA structure upon complexation with ruthenium complexes [16,40,50,51].

We measure the evolution of RDC solution CD signal with increasing the DNA base pairs concentration. A series of spectra, obtained for RDC37Cl, are shown in fig. 8. The RDC solution does not exhibit circular dichroism because the solution is racemic. Adding amounts of DNA, CD signal develops, both due to the DNA chirality itself, to its change upon complexation with RDC, and also due to the change of composition of the free RDC solution, which is no longer racemic. The same titration as the absorption titration is performed : DNA is progressively added to a RDC solution. We observe that several circular dichroism bands appear on the spectrum during the titration of RDC solution by DNA base pairs. At very low values of DNA base pairs concentration, negative bands around 250nm and 275nm develop and a positive band around 260nm appear. At high values, we observe a very similar characteristic spectrum of DNA alone with negative band at 250nm and positive band at 275nm.

We thus follow the evolution of the height of the CD signal measured at 250 nm as a function of the complexation ratio, ν^D, obtained from the light absorption measurements (fig. 9). For all studied RDCs, two different regimes appear. At low complexation ratios, the circular dichroism at 270 nm strongly increases. Then a change of slope is observed at larger complexation ratios, and further complexation does not lead to an increase of the overall CD signal. For RDC37Cl, the crossover complexation ratio between the two regimes corresponds to ν_c^D obtained from absorbance measurements (fig. 9a and c). For RDC40Cl (fig. 9b), the two regimes are also observed, which validates our hypothesis of two absorption modes identical molar extinction ratio. We thus conclude that, for the two different RDC studied, the two modes of association induce different change of chirality. The compound $Ru(bpy)_2dppz^{2+}$ shows the same behaviour of RDC for the circular dichroism

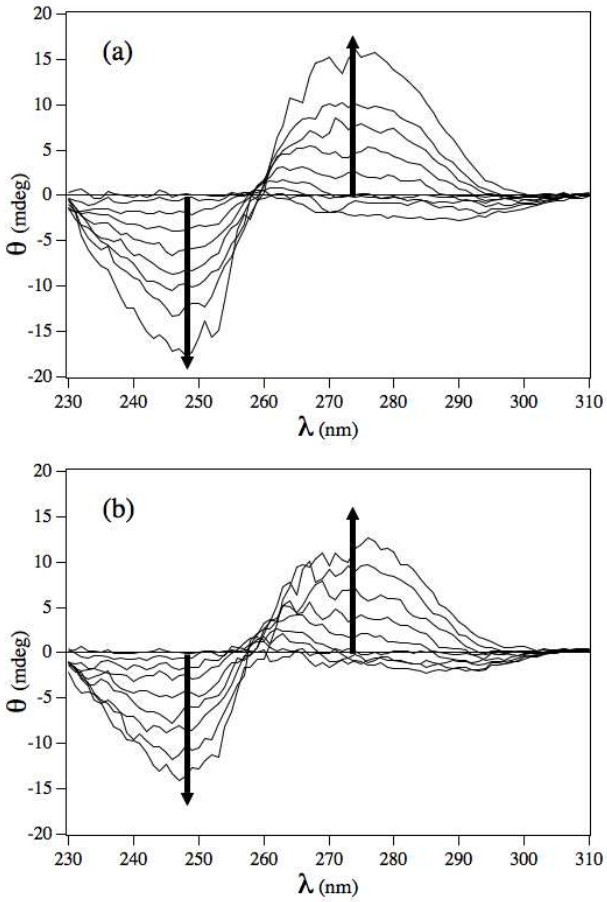

Fig. 8 Ellipticity of DNA/RDC complex as a function of DNA base pairs concentration for RDC37Cl **(a)** and RDC40Cl **(b)**. Measurements are performed for $L_t = 2\text{x}10^{-5}M$ and $\frac{D_t}{L_t}$ values equal to 0.5, 1, 2, 3, 5 and 8. Arrows indicate the evolution of the curves when DNA base pairs concentration increases.

experiments (fig. 10). According to the litterature [19], intercalation leads to a great structural modification of the DNA macromolecule (increasing the distance between two base pairs of the order of 3.4 $\AA$) and so the ellipticity is modified. During the titration, the ellipticity increases a lot in the first domain (intercalation), this variation would be the same for the different intercalation geometries cited before (partial, total, quasi-intercalation). For the second domain, the variation of the ellipticity is weak and cannot be attributed to an intercalation.

4.2 Absorption into saline medium

To characterize the second mode we perform the same absorption spectrophotometry as before changing the salt concentration medium to 40 mM in sodium chloride. We limit

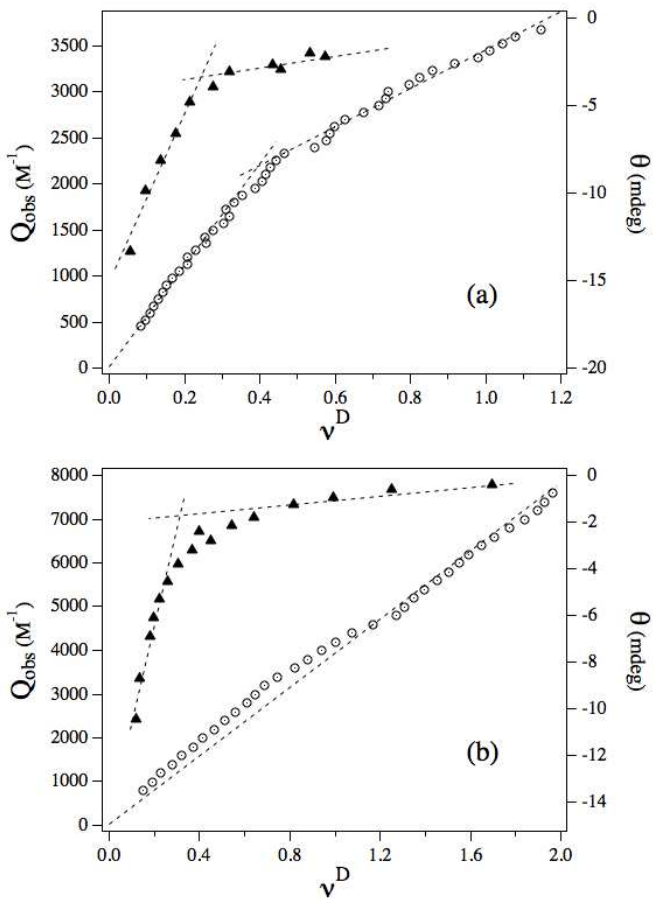

Fig. 9 Evolution of the absorbance *per* mole of DNA, Q^D_{obs} (empty circles, left scale) and of the ellipticity, θ (filled triangles, right scale), as a function of the adsorption ratio ν^D, for RDC37Cl **(a)** and RDC40Cl **(b)**. Dashed lines are guides to the eye.

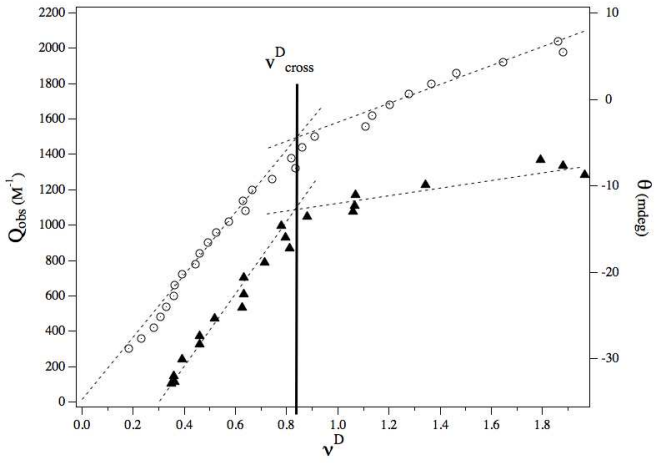

Fig. 10 Evolution of the absorbance *per* mole of DNA, Q^D_{obs} (empty circles, left scale) and of the ellipticity, θ (filled triangles, right scale), as a function of the adsorption ratio ν^D, for $Ru(bpy)_2(dppz)^{2+}$. Dashed lines are linear fits at small and large ν^D values.

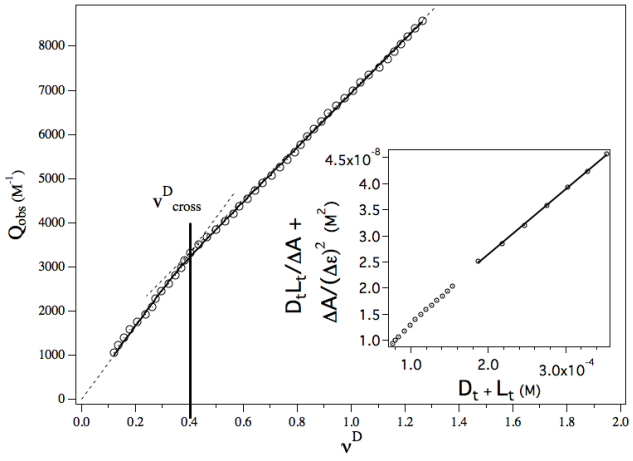

Fig. 11 Evolution of Q^D_{obs} as a function of the fraction of occupied DNA base pairs, ν^D for RDC37Cl in a 40 *mM* of sodium chloride solution. Dashed lines are linear fits of the asymptotic behaviors at low and high ν^D from eq. 11. Thick continuous lines are fits according to eq. 13 with K_{a2}/K_{a1} as the sole fitting parameter. *Insert* : Hildebrand-Benesi[39] plot of the evolution of the absorbance as a funciton of the total concentration of ligands and base pairs, according to eq. 17 for $n = 5$ iterations. The slope leads to $\Delta\varepsilon_1$ and one deduces K_{a1} from the value at origin.

our study to the *RDC*37*Cl* compound, the one with the most biological interest. Results are given in fig. 11. The general behaviour is the same : we observe two domains corresponding to two different association modes. Using the methods described above we determine the caracteristic values and observe that the K_{a1} and ε_{b1} (from the two methods) values are the same. Comparing the K_{a1} values without and with salt we get approximately the same one : 5.9x10^4 M^{-1} and 8x10^4 M^{-1}. This observation is reasonable because the ionic force is not involved in the free enthalpy of the formed complex. The free enthalpy variation is essentially due to π-stacking interactions between complexes ligands and DNA base pairs. Moreover, the ε_{b2} values are very similar with or without salt.

On the other side, we observe a decrease of one order of magnitude of the affinity of the ligand with DNA (from $K_{a2} =$ 3.5x10^3 M^{-1} whithout salt to 4.8x10^2 M^{-1} with 40 *mM* of salt). The concentration of counterions in the absence of *NaCl* is 0.12 mM. The evolution of the affinity as a function of the salt concentration c_{NaCl} may be described by the Manning's theory[52,53] and one has :

$$\ln K_a = \ln K_a^0 - z\Psi \ln c_{NaCl} \qquad (18)$$

where K_a^0 is the binding constant corrected for the the free energy of ion release, z the valency of the complexing ions and $\Psi = 0.88$ is the fraction of counterions associated with each DNA phosphate. The measured slope of the affinity is lower than 0.88 and is equal to 0.34. Such a discrepancy has already observed for tris(phenanthroline)Ru(II) binding to DNA and could arise from change in ligand or ligand hydration upon binding[25].The magnitude of K_a^0 indicates the contribution of non-electrostatic forces to the interaction. We have : $K_a^0 = 1.6\text{x}10^2$ M^{-1}, indicating that, in the absence of added sodium chloride, the interaction is largely dominated by the electrostatic contribution whereas at 40 mM of sodium chloride, the free enthalpy associated to the electrostatic interaction is equal to 82 % of the total free enthalpy of interaction. DNA structure exhibits well-defined sites for cations binding[54]. Many cations have been shown to condense onto DNA[55–57], as well as positively charged proteins[58–60]. Depending on their size and valency, cations may bind preferentially in DNA grooves or DNA strands[61]. Due to the large contribution of the nonelectrostatic interactions at high ionic strength, we may assume that at least some part of the ruthenium complex is localized in the DNA grooves. The structure of the DNA/RDC complex may moreover change when the ionic strength is varied, and structural experiments or numerical simulations would be required for a complete description of the structure associated to this mode of interaction.

5 Conclusion

Our results demonstrate the remarkable ability of DNA to accept high density binding of organometallic ligands, where one DNA base pair is complexed by more than one organometallic molecule. At high complexation ratios, the complexation of DNA by the ligands implies two different sites along the DNA chain. The most affine interaction involves intercalation of one of the ligand in between DNA base pairs. We have measured the enthalpy of association of RDC37Cl in this mode (data not shown), and found $\Delta H = 6.52$ kcal.mol^{-1}, slightly larger than the enthalpy of association of $Ru(phen)_2 dppz^{2+}$ (5.2 kcal.mol^{-1}), that is mainly due to the intercalation of the dppz ligand between DNA base pairs[62]. The other complexation mode involves electrostatic interaction, and may be due to the adsorption of the ruthenium compound onto the DNA surface. The least affine complexation sites are still available while intercalation is already performed. These results shed a new light on the interaction mechanisms of DNA with organometallic compounds, and show that new structures of DNA/organometallic compounds may be reached at complexations ratios larger than one complexant *per* DNA base pair.

6 Appendix

6.1 Description of the model

Let us consider that two different association sites compete for the association of DNA with the studied RDC. This model is characterized by two association sites S_1 and S_2 with the affinity constants K_{a1} and K_{a2} :

$$\text{S}_1 + \text{RDC} \underset{K_{a1}}{\rightleftharpoons} (\text{S}_1 - \text{RDC}) \text{ with } K_{a1} = \frac{L_{b1}}{S_{f1} L_f}$$
$$\text{S}_2 + \text{RDC} \underset{K_{a2}}{\rightleftharpoons} (\text{S}_2 - \text{RDC}) \text{ with } K_{a2} = \frac{L_{b2}}{S_{f2} L_f}$$

L_{b1} and L_{b2} being the concentrations of ligands bounds to association sites 1and 2, L_f the concentration of free ligands and S_{f1} and S_{f2} the concentrations of free sites.

The mass conservation laws are :

$$S_{t1} = S_{f1} + L_{b1} \quad (19a)$$
$$S_{t2} = S_{f2} + L_{b2} \quad (19b)$$
$$L_t = L_f + L_{b1} + L_{b2} \quad (19c)$$

where $S_{t1} = \phi_1 S_t$ and $S_{t2} = \phi_2 S_t$ are the numbers of sites of type 1 and 2, ϕ_1 and ϕ_2 being the fractions of sites 1 and 2 along the DNA double strand. The fraction of DNA occupied sites is now given by :

$$\nu^S = \frac{L_{b1} + L_{b2}}{S_t} \quad (20)$$

6.2 Expression of Q_{obs}

We need to evaluate the fraction of ligands bound to the first or the second site kinds, L_{b1}/L_{b2}. Let us first consider the conservation of adsorption sites of type 1 and 2.

$$S_{t1} = S_{f1} + L_{b1} = \phi_1 S_t = \phi_1 \frac{L_{b1} + L_{b2}}{\nu^S} \quad (21a)$$
$$S_{t2} = S_{f2} + L_{b2} = \phi_2 S_t = \phi_2 \frac{L_{b1} + L_{b2}}{\nu^S} \quad (21b)$$

Eq. 20 has been used to derive the last equalities.

The mass actions laws impose :

$$\frac{K_{a2}}{K_{a1}} = \frac{L_{b2}}{L_{b1}} \frac{S_{f1}}{S_{f2}} \quad (22)$$

The expressions of S_{f1} and S_{f2} are obtained from eq. 21 :

$$\frac{S_{f1}}{L_{b1}} = \frac{\phi_1}{\nu^S} \left(1 + \frac{L_{b2}}{L_{b1}}\right) - 1 \quad (23a)$$
$$\frac{S_{f2}}{L_{b1}} = \frac{\phi_2}{\nu^S} \left(1 + \frac{L_{b2}}{L_{b1}}\right) - \frac{L_{b2}}{L_{b1}} \quad (23b)$$

Thus,

$$\frac{L_{b2}}{L_{b1}}\frac{K_{a1}}{L_{a2}} = \frac{\frac{\phi_2}{\nu^S}\left(1+\frac{L_{b2}}{L_{b1}}\right)-\frac{L_{b2}}{L_{b1}}}{\frac{\phi_1}{\nu^S}\left(1+\frac{L_{b2}}{L_{b1}}\right)-1} \tag{24}$$

leading to the following equation for L_{b2}/L_{b1} :

$$\phi_1\left(\frac{L_{b2}}{L_{b1}}\right)^2 - \left(\frac{K_{a2}}{K_{a1}}(\phi_2-\nu^S)-\phi_1+\nu^S\right)\frac{L_{b2}}{L_{b1}} - \phi_2\frac{K_{a2}}{K_{a1}} = 0 \tag{25}$$

from which L_{b2}/L_{b1} is obtained as a function of ν^S. The variation of absorbance per mole of DNA, Q^S_{obs} can thus be written :

$$\begin{aligned} Q^S_{obs} &= \frac{A_{obs}-\varepsilon_f L_t}{S_t} && \text{(26a)}\\ &= \frac{\varepsilon_f L_t - (\varepsilon_f L_f + \varepsilon_{b1}L_{b1}+\varepsilon_{b2}L_{b2})}{S_t} && \text{(26b)}\\ &= \nu^S(\varepsilon_f-\varepsilon_{b2}) + \frac{L_{b1}}{S_T}(\varepsilon_{b2}-\varepsilon_{b1}) && \text{(26c)}\\ &= \nu^S(\varepsilon_f-\varepsilon_{b2}) + \frac{\nu^S}{1+\frac{L_{b2}}{L_{b1}}(\nu^S)}(\varepsilon_{b2}-\varepsilon_{b1}) && \text{(26d)} \end{aligned}$$

L_{b2}/L_{b1} being the positive root of eq. 25. $Q^S_{obs}(\nu^S)$ is plotted in fig. 12 for different values of K_{a2}/K_{a1}, using the values of the absorption coefficients obtained from the analysis of the slope of the esperimental measures Q^S_{obs}. We check that Q^S_{obs} is an increasing function of ν^S. As a consequence, the relationship between Q^S_{obs} and ν^S is monovalent and the method developed for the case of a single equilibrium may be used in our situation. From this relation, we obtain the evolution of Q^D_{obs} with the fraction of occupied base pairs, ν^D. Let indeed be p_1 and p_2 the number of base pairs in sites 1 and 2. The fraction of occupied base pairs, ν^D is related to ν^S by :

$$\nu^D = (p_1\phi_1 + p_2\phi_2)\nu^S = \langle p\rangle \nu^S \tag{27}$$

where $\langle p\rangle$ is the weighted average of p_1 and p_2. We thus obtain, by dividing by $\langle p\rangle$:

$$Q^D_{obs} = \nu^D(\varepsilon_f-\varepsilon_{b2}) + \frac{\nu^D}{1+\frac{L_{b2}}{L_{b1}}\left(\frac{\nu^D}{\langle p\rangle}\right)}(\varepsilon_{b2}-\varepsilon_{b1}) \tag{28}$$

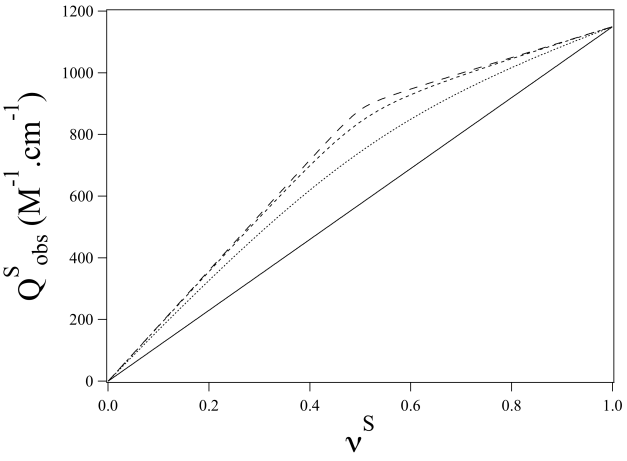

Fig. 12 Theoretical evolution of Q^S_{obs} as a function of ν^S. The curves are computed using eq. 26 with molar absorbance values obtained for RDC37Cl : $\varepsilon_f = 12550$, $\varepsilon_{b1} = 6293$ and $\varepsilon_{b2} = 10858$ $mol^{-1}.l.cm^{-1}$. From top to bottom, $K_{a2}/K_{a1} = 10^{-3}, 10^{-2}, 10^{-1}$ and 1.

Acknowledgements

The authors acknowledge financial support from the ANR PhotoBioMet project. E. Ennifar is thanked for his help in the calorimetric measurements.

References

1 B. Rosenberg, L. VanCamp and T. Krigas, *Nature*, 1965, **205**, 698–699.
2 S. E. Shermann, D. Gibson, A. H.-J. Wang and S. J. Lippard, *Science*, 1985, **230**, 412–417.
3 B. Rosenberg, L. VanCamp, E. B. Grimley and A. J. Thomson, *J. Biol. Chem.*, 1967, **242**, 1347.
4 M. Clarke and M. Stubbs, *Metallopharceuticals and DNA*, 1996, vol. 32, pp. 727–780.
5 M. Clarke, *Electron transfer reactions : inorganic, organometallic, and biological applications, Advances in Chemistry Series*, 1997, **253**, 343–365.
6 G. Sava, *Clin. Cancer Res.*, 2003, **9**, 1898–1905.
7 C. G. Hartinger, M. A. Jakupec, S. Zorbas-Siefried, M. Groessl, A. Egger, W. Berger, P. J. Dyson and B. K. Keppler, *Chem. Biodivers.*, 2008, **5**, 2140–2155.
8 L. Leyva, C. Sirlin, L. Rubio, C. Franco, R. L. Lagadec, J. Spencer, P. Bischoff, C. Gaiddon, J. P. Loeffler and M. Pfeffer, *Eur. J. Inorg. Chem*, 2007, 3055–3066.
9 Y. Jenkins, A. E. Friedman, N. J. Turro and J. K. Barton, *Biochemistry*, 1992, **31**, 10809–10816.
10 E. Ruba, J. R. Hart, and J. K. Barton, *Inorg. Chem.*, 2004, **43**, 4570–4578.
11 G. Yang, J. Z. Wu, L. Wang, L. N. Ji and X. Tian, *J. Inorg. Biochem.*, 1997, **66**, 141–144.
12 J. K. Barton, J. M. Goldberg, C. V. Kumar and N. J. Turro, *J. Am. Chem. Soc*, 1986, **108**, 2081–2088.
13 R. M. Hartshorn and J. K. Barton, *J. Am. Chem. Soc*, 1992, **114**, 5919–5925.

14 M. Klajner, P. Hébraud, C. Sirlin, C. Gaiddon and S. Harlepp, *J. Phys. Chem. B*, 2010, **114**, 14041–14047.

15 E. Grueso, G. López-Pérez, M. Castellano and R. Prado-Gotor, *J. Inorg. Biochem.*, 2012, **106**, 1–9.

16 P. Lincoln and B. Norden, *J. Phys. Chem. B*, 1998, **102**, 9583–9594.

17 L. Hu, Z. Bian, H. Li, S. Han, Y. Yuan, L. Gao, and G. Xu, *Anal. Chem.*, 2009, **81**, 9807–9811.

18 A. Mihailovic, I. Vladescu, M. McCauley, E. Ly, M. C. Williams, E. M. Spain and M. E. Nunez, *Langmuir*, 2006, **22**, 4699–4709.

19 I. D. Vladescu, M. J. McCauley, M. E. Nunez, I. Rouzina and M. C. Williams, *Nat. Methods*, 2007, **4**, 517.

20 V. V. Kostjukov, A. A. Santiago, F. R. Rodriguez, S. R. Castilla, J. A. Parkinson and M. P. Evstigneev, *Phys. Chem. Chem. Phys.*, 2012, **14**, 5588–5600.

21 W. Treesuwan, K. Wittayanarakul, N. G. Anthony, G. Huchet, H. Alniss, S. Hannongbua, A. I. Khalaf, C. J. Suckling, J. A. Parkinson and S. P. Mackay, *Phys. Chem. Chem. Phys.*, 2009, **11**, 10682–10693.

22 G. Scatchard, *Ann. N. Y. Acad. Sci.*, 1949, **51**, 660–672.

23 J. D. McGhee and P. H. V. Hippel, *J. Mol. Biol.*, 1974, **86**, 469–489.

24 L.-H. Guo, M.-Y. Wei and H. Chen, *J. Phys. Chem. B*, 2006, **110**, 20568–20571.

25 S. Satyanarayana, J. C. Dabrowiak and J. B. Chaires, *Biochemistry*, 1992, **31**, 9319–9324.

26 D. Z. M. Coggan, I. S. Haworth, P. J. Bates, A. Robinson and A. Rodger, *Inorg. Chem.*, 1999, **38**, 4486–4497.

27 M.-J. Han, Z.-M. Duan, Q. Hao, S.-Z. Zheng and K.-Z. Wang, *J. Phys. Chem. B*, 2007, **111**, 16577–16585.

28 S. A. Tysoe, R. J. Morgan, A. D. Baker and T. C. Strekas, *J. Phys. Chem. B*, 1993, **97**, 1707–1711.

29 B. H. Yun, J.-O. Kim, B. W. Lee, P. Lincoln and B. Norden, *J. Phys. Chem. B*, 2003, **107**, 9858–9864.

30 L. Fetzer, B. Boff, M. Ali, M. Xiangjun, J.-P. Collin, C. Sirlin, C. Gaiddon and M. Pfeffer, *Dalton Trans.*, 2011, **40**, 8869–8878.

31 I. Joliffe, *Principle Component Analysis*, Springer Verlag, 2nd Ed., 2002.

32 C. J. Halfman and T. Nishida, *Biochemistry*, 1972, **11**, 3493–3498.

33 W. Bujalowski and T. M. Lohman, *Biochemistry*, 1987, **26**, 3099–3106.

34 A. Ryabov, V. Sukharev, L. Alexandrova, R. L. Lagadec and M. Pfeffer, *Inorg. Chem.*, 2001, **40**, 6529–6532.

35 E. Amouyal, A. Homsi, J.-C. Chambron and J.-P. Sauvage, *J. Chem. Soc. Dalton Trans.*, 1990, 1841–1845.

36 B. P. Sullivan, D. J. Salmon and J. Meyer, *Inorg. Chem.*, 1978, **17**, 3334–3341.

37 R. O. S. Diaz, R. L. Lagadec and A. D. Ryabov, *J. Biol. Inorg. Chem*, 2013, **18**, 547–555.

38 S. Bonnet, J. Li, M. A. Siegler, L. S. von Chrzanowski, A. L. Spek, G. van Koten and R. J. M. K. Gebbink, *Chem. Eur. J.*, 2009, **15**, 3340–3343.

39 H. Benesi and J. Hildebrand, *J. Am. Chem. Soc*, 1949, **71**, 2703–2707.

40 C. Hiort, B. Norden and A. Rodger, *J. Am. Chem. Soc*, 1990, **112**, 1971–1982.

41 K. Gisselfalt, P. Lincoln, B. Norden and M. Jonsson, *J. Phys. Chem. B*, 2000, **104**, 3651–3659.

42 C. G. Coates, J. J. McGarvey, P. L. Callaghan, M. Coletti and J. G. Hamilton, *J. Phys. Chem. B*, 2001, **105**, 730–735.

43 M. Eriksson, M. Leijon, C. Hiort, B. Norden and A. Graslund, *Biochemistry*, 1994, **33**, 5031–5040.

44 A. Greguric, I. D. Greguric, T. W. Hambley, J. R. Aldrich-Wright and J. G. Collins, *J. Chem. Soc. Dalton Trans.*, 2002, 849–855.

45 W. Chen, C. Turro, L. A. Friedman, J. K. Barton and N. J. Turro, *J. Phys. Chem. B*, 1997, **101**, 6995–7000.

46 A. E. Friedman, J.-C. Chambron, J.-P. Sauvage, N. J. Turro and J. K. Barton, *J. Am. Chem. Soc*, 1990, **11**, 4960–4962.

47 J. K. Barton, A. T. Danishefsky and J. M. Goldberg, *J. Am. Chem. Soc*, 1984, **106**, 2172–2176.

48 S. Satyanarayana, J. C. Dabrowiak and J. B. Chaires, *Biochemistry*, 1993, **32**, 2573–2584.

49 O. Mauffret, M. Monnt, M. Lanson, J. Armier and S. Fermandjian, *Biochem. Biophys. Res. Commun.*, 1989, **165**, 602–614.

50 C. Hiort, P. Lincoln and B. Norden, *J. Am. Chem. Soc*, 1993, **115**, 3448–3454.

51 P. Lincoln, E. Tuite and B. Norden, *J. Am. Chem. Soc*, 1997, **119**, 1454–1455.

52 G. S. Manning, *J. Chem. Phys.*, 1969, **51**, 924–933.

53 M. T. Record, C. Anderson and T. Lohman, *Q. Rev. Biophys.*, 1978, **11**, 103–178.

54 A. A. Kornyshev, D. J. Lee, S. Leikin and A. Wynveen, *Rev. Mod. Phys.*, 2007, **79**, 943–996.

55 J. Widom and R. L. Baldwin, *Biopolymers*, 1983, **22**, 1595–1620.

56 V. Bloomfield, *Biopolymers*, 1991, **31**, 1471–1481.

57 L. C. Gosule and J. A. Schellman, *Nature*, 1976, **259**, 333–334.

58 J. DeRouchey, R. Netz and J. Raedler, *Eur. Phys. J. E.*, 2005, **16**, 17–28.

59 J. DeRouchey, V. A. Parsegian and D. C. Rau, *Biophys. J.*, 2010, **99**, 2608–2615.

60 M. W. Hsiang and R. D. Cole, *Proc. Nat. Acad. Sci. USA*, 1977, **74**, 4852–4856.

61 A. G. Cherstvy, *Phys. Chem. Chem. Phys.*, 2011, **13**, 9942–9968.

62 I. Haq, P. Lincoln, D. Suh, B. N. B. Z. Chowdhry and J. B. Chaires, *J. Am. Chem. Soc*, 1995, **117**, 4788–4796.

Contents page figure

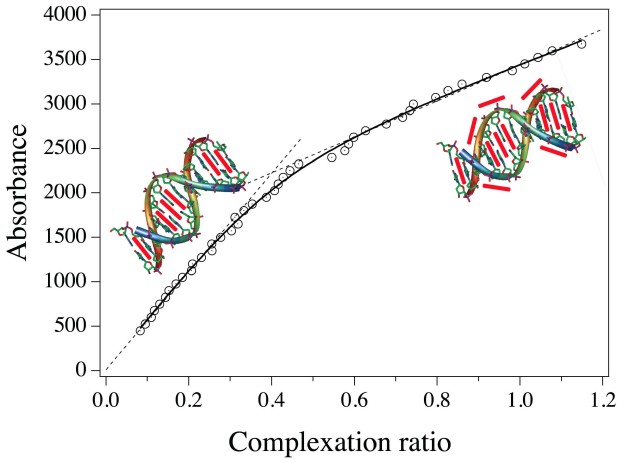

Fig. 13 Organometallic compounds possess two modes of interaction with DNA : intercalation at low complexation ratios and electrostatic adsorption at high ratio.